JACS
JOURNAL OF THE AMERICAN CHEMICAL SOCIETY
pubs.acs.org/JACS
Article

Mitigating Succinonitrile–Li Molecular Crosstalk in In Situ Polymerization toward High-Voltage and Low-Temperature Solid-State Li Metal Batteries

Shuai Liu, Rujian Fu, Mengfan Zhao, Bao Li, Xueqing Chen, Lifeng Hou,* Shi Wang,* Zhong Jin,* and Qian Wang*

Cite This: J. Am. Chem. Soc. 2026, 148, 24499–24509
Read Online
ACCESS | Metrics & More | Article Recommendations | Supporting Information

ABSTRACT: In situ polymerization technology presents a promising avenue for constructing solid-state Li metal batteries with tight electrode–electrolyte interfacial contact. However, its application is often compromised by slow Li^+ kinetics at low temperatures and poor stability against high-voltage cathodes. While succinonitrile (SN) has been introduced as a plasticizer to enhance ionic conductivity and oxidation resistance, it exhibits high reactivity toward Li metal, causing continuous side reactions and an unstable interface. Herein, we propose a methoxy-functionalized strategy to address the SN–Li molecular crosstalk by methoxylating one terminal of SN, resulting in 3-methoxypropionitrile (MPN), which is incorporated into an in situ polymerized poly(1,3,5-trioxane) electrolyte. Among them, the methoxy group introduces a weakly positive dipole via its C–H bond, which not only significantly lowers the freezing point to −62.9 °C, much lower than that of SN (50 °C), resulting in enhanced low-temperature kinetics, but also limits anion mobility and further enhances Li^+ kinetics through ion–dipole interactions with $TFSI^-$ anions. Simultaneously, the electron-withdrawing cyano group is retained, endowing the electrolyte with high oxidation resistance and a stability window exceeding 5.0 V. Therefore, the obtained solid-state electrolyte exhibits a high ionic conductivity (0.9×10^{-3} S cm^{-1}) and a high Li^+ transfer number of 0.70 at −20 °C. As a result, the Li||$LiFePO_4$ full cells can run stably and deliver high capacity retention (~100%) after 1500 cycles at 10 C. Additionally, all the full cells (Li||LFP, Li||NCM811, Li||NCM622 (high loading: 25.27 mg cm^{-2}), and Li||LCO (cutoff voltage: 4.5 V)) can run stably at −20 °C and even −40 °C with high capacity retention. This work offers a feasible molecular functionalization strategy to overcome the interfacial incompatibility of traditional plasticizers in solid-state Li metal batteries, advancing their practical application.

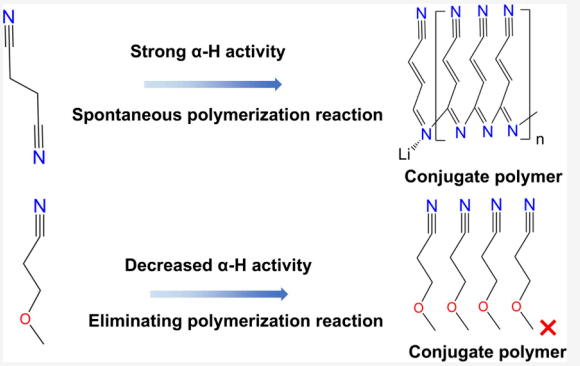

INTRODUCTION

Lithium-ion batteries (LIBs) have revolutionized modern energy storage systems and have become the cornerstone of portable electronics and electric vehicles owing to their high energy density, long cycle life, and competitive operating voltage.[1−3] However, the energy density of conventional LIBs based on graphite anodes is approaching the theoretical limit, making LIBs increasingly inadequate for meeting the growing energy demands.[4,5] Recently, Li metal batteries (LMBs), which utilize Li metal as the anode to achieve significantly higher energy density, have garnered considerable interest.[6,7] Nevertheless, the high reactivity of the Li metal anode promotes continuous side reactions with liquid electrolytes, resulting in the formation of an unstable solid electrolyte interphase (SEI).[8] This fragile SEI layer is prone to fracture during repeated cycling, enhancing localized Li^+ flux and facilitating Li-dendrite growth, thereby deteriorating cycling stability and exacerbating safety risks.[9−11]

To address these challenges, developing new solid polymer electrolytes (SPEs) to replace traditional liquid electrolytes has emerged as a promising strategy, such as polyoxides (e.g., poly(ethylene oxide), PEO),[12] poly(propylene carbonate) (PC),[13] poly(1,3-dioxolane) (poly-DOL),[14] poly(vinylidene fluoride) (PVDF),[15] etc., gaining widespread attention due to their flexibility, ease of processing, and enhanced safety without leakage risks. Nevertheless, most SPEs still face limitations, such as low ionic conductivity and poor interfacial contact, significantly impeding Li^+ transport kinetics, thereby limiting

Received: April 8, 2026
Revised: May 6, 2026
Accepted: May 12, 2026
Published: June 4, 2026

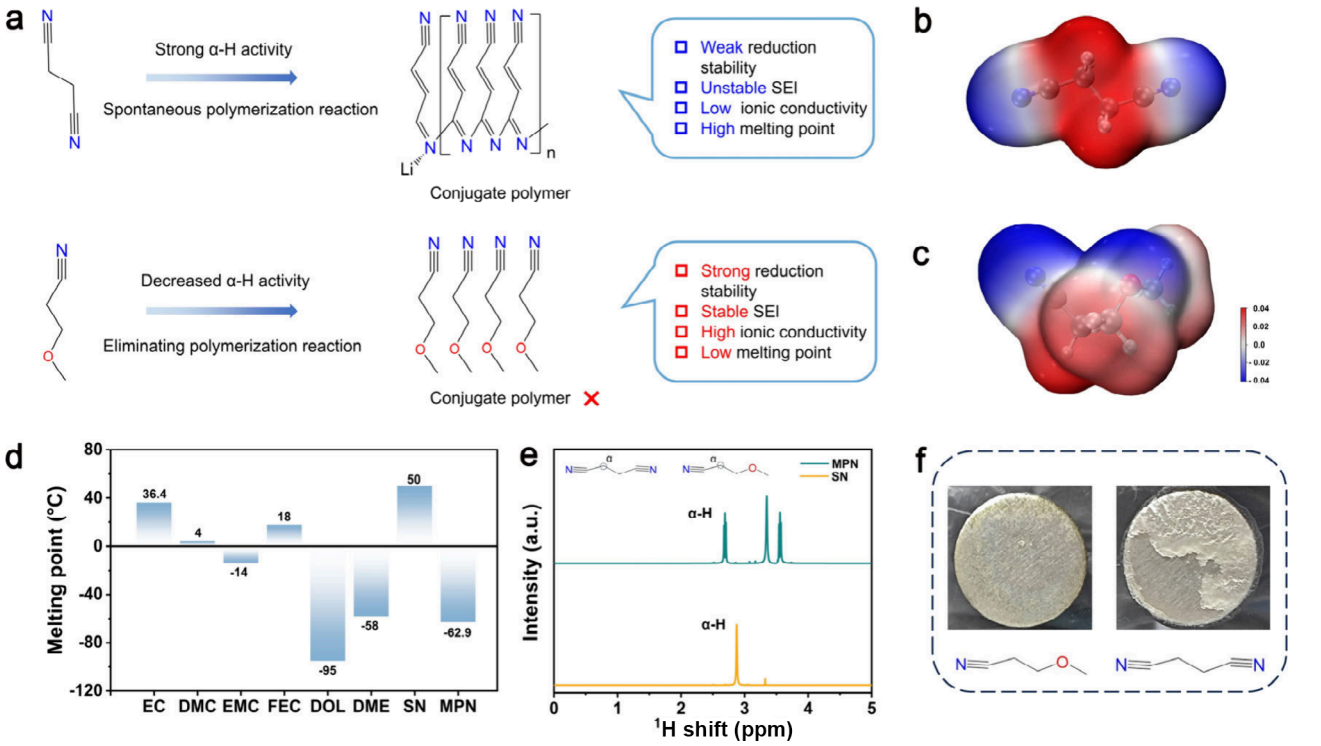

Figure 1. Solvent molecule design and electrochemical stability. (a) Chemical structure design of SN and MPN solvent molecules and their related properties. (b, c) ESP distribution of different solvents, (b) SN and (c) MPN. (d) Freezing point distribution of different ester solvents, ether solvents, and MPN and SN. (e) ^{1}H NMR spectra of SN and MPN. (f) Optical images of SN and MPN dissolved in TXE on the surface of Li metal.

their applicability under high-rate operation and in low-temperature environments.[16−18]

In situ polymerization has recently been developed as an effective strategy to construct intimate electrode−electrolyte interfaces and enhance interfacial compatibility.[19] This technique allows liquid precursors to permeate porous electrodes thoroughly before polymerization, resulting in reduced interfacial resistance and improved ion transport pathways.[20,21] Despite these advantages, in situ polymerization often leads to the formation of long-chain polymers due to continuous polymerization reactions during the electrochemical process, resulting in reduced ionic conductivity and compromised Li^+ transport.[22,23] Moreover, current mainstream ring-opening polymerization electrolytes, e.g., poly-DOL, are susceptible to oxidative decomposition at high voltage, resulting in an unstable and overly thick cathode electrolyte interphase (CEI), along with their low ionic conductivity—all of which contribute to poor cycling performance.[24,25]

To enhance the oxidative stability and ionic conductivity of in situ formed SPEs, succinonitrile (SN) is usually introduced as a plasticizer to suppress polymer chain crystallization, improve ion conduction, and enhance high-voltage stability.[26] However, SN exhibits high reactivity toward Li metal, primarily due to the electron-withdrawing cyano groups (—C≡N) that activate α-H, which induces continuous interface corrosion and side reactions, hindering its further application in solid-state LMBs.[27,28] Several approaches have been proposed to mitigate the incompatibility between SN and Li metal, such as constructing artificial SEI layers or encapsulating SN molecules within cross-linked polymer networks.[29−32] While these methods alleviate side reactions to some extent, they fail to address the fundamental molecular instability of SN, underscoring the need for innovative molecular design.

In this work, we propose a terminal functionalization strategy to molecularly modulate the reactivity of SN. By methoxylating one terminal nitrile group of SN, we obtain 3-methoxypropionitrile (MPN), which is introduced into an in situ polymerized poly(1,3,5-trioxane) (PTXE)-based SPE. The introduced methoxy group ($-OCH_3$) provides a weakly positive dipole that interacts with anions via ion−dipole interactions, thereby limiting anion mobility and promoting Li^+ transference kinetics. Meanwhile, the preserved cyano group inhibits the loss of lone pair electrons from the ether oxygen and endows the electrolyte with high oxidation stability, achieving an operational voltage window exceeding 5.0 V. Thus, the designed SPE demonstrates high ionic conductivity (0.9×10^{-3} S cm^{-1}) and a Li^+ transference number of 0.70 even at −20 °C. At room temperature, Li||$LiFePO_4$ cells maintain nearly 100% capacity after 1500 cycles at 10 C. Even when the temperature drops to −20 °C, Li||Li symmetric cells can cycle stably for over 1000 h, and Li||NCM811 full cells display >80% capacity after 500 cycles. This molecular engineering strategy provides a feasible pathway to address interfacial instability in plasticized SPEs and facilitates the development of high-voltage and low-temperature solid-state LMBs.

RESULTS AND DISCUSSION

Molecular Innovation and Electrolyte Design

SN serves as an efficient solid-state plasticizer, featuring a solid crystalline form with negligible vapor pressure, high Li salt solvation ability, and strong antioxidant resistance under high voltages. These properties collectively help reduce polymer crystallinity, enhance ionic conductivity, and broaden the electrochemical window in in situ polymerized SPEs. To alleviate the side reactions between it and the Li metal anode,

https://doi.org/10.1021/jacs.6c07280
J. Am. Chem. Soc. 2026, 148, 24499−24509

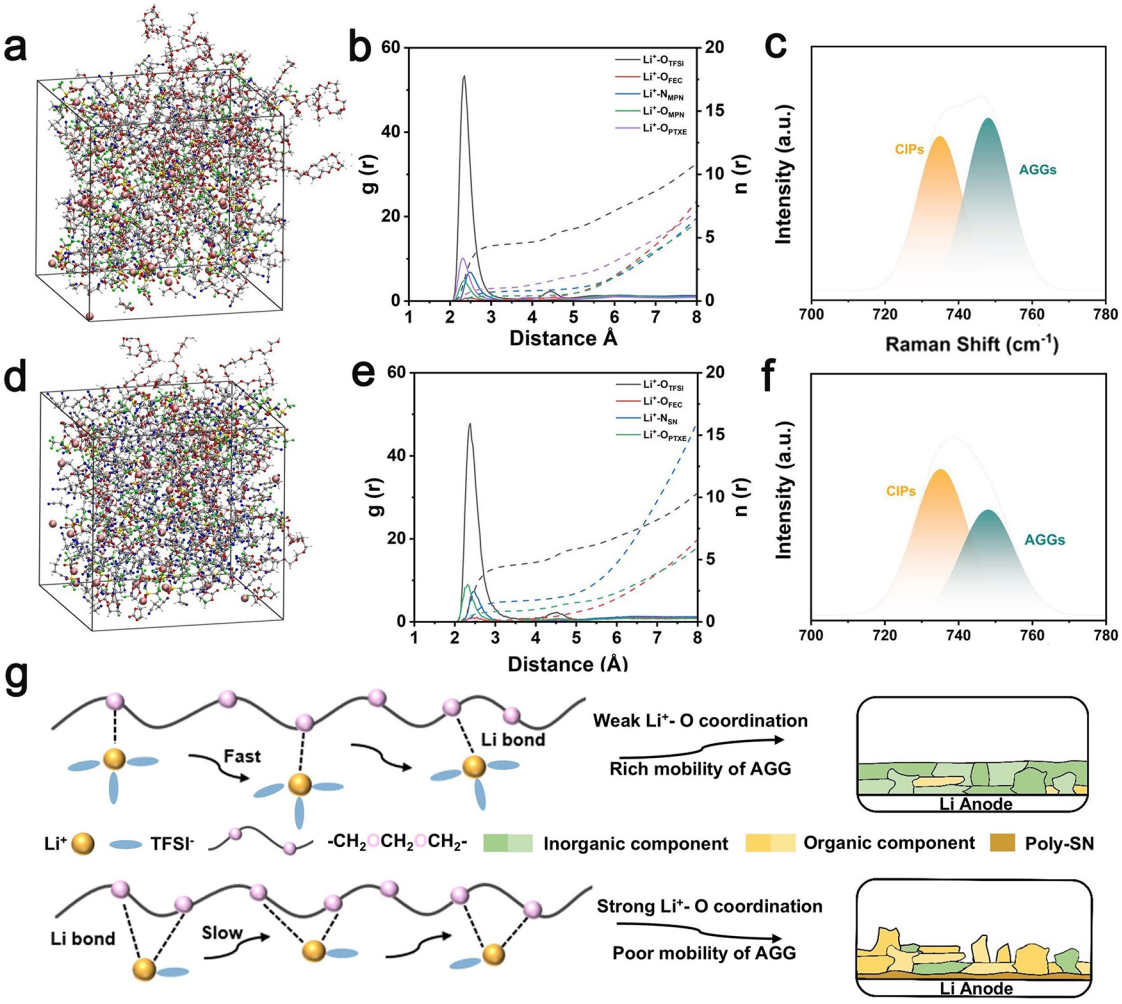

Figure 2. Migration mechanism of Li^+ in SPEs. (a) Molecular dynamics simulation snapshot of MPN-PTXE SPE. (b) Radial distribution functions and coordination numbers of MPN-PTXE SPE. (c) Raman spectra of MPN-PTXE SPE. (d) Molecular dynamics simulation snapshot of SN-PTXE SPE. (e) Radial distribution functions and coordination numbers of SN-PTXE SPE. (f) Raman spectra of SN-PTXE SPE. (g) Transport pathways of Li^+ in MPN-PTXE SPE and SN-PTXE SPE.

we modified one terminal of SN by introducing a methoxy group, yielding 3-methoxypropionitrile (MPN). As shown in Figure 1a, the $-OCH_3$ group, serving as an electron-donating group, elevated the electron density around the α-hydrogen, thereby stabilizing it and reducing its propensity for self-polymerization catalyzed by the Li metal anode. At the same time, the $-OCH_3$ group exhibited the favorable compatibility of ether-based molecules with Li metal, and the preserved —C≡N group retained the high oxidation resistance of cyano-based electrolytes for cathodes under high voltages. Subsequently, we analyzed the electrostatic potential (ESP) of SN and MPN molecules. As shown in Figure 1b,c, the negative charge in SN was predominantly localized on the N atom. In contrast, MPN exhibited a delocalization of negative charge between the O and N atoms, suggesting reduced reactivity. MPN possesses electron-attracting $-CH_3$ groups (red regions). The introduction of $-CH_3$ groups promotes attack on anions. Through ion−dipole interactions with anions, this restricts anion mobility while enhancing Li^+ mobility.[33] Although the $-OCH_3$ group in MPN possessed lone pair electrons that could potentially lead to oxidation, the strong electron-withdrawing nature of the —C≡N group mitigated this effect. This complementary electronic structure positioned MPN as a highly promising candidate for replacing SN in SPEs. Furthermore, the introduction of the $-OCH_3$ significantly depressed the melting point of MPN to −62.9 °C, far below that of SN (50 °C) and common electrolyte molecules, underscoring its exceptional suitability for low-temperature application (Figure 1d).

Then, the MPN molecule was introduced into the in situ polymerized PTXE systems to achieve a high-performance SPE, named MPN-PTXE. As shown in Figure S1, the SPE was synthesized via the ring-opening polymerization of 1,3,5-trioxane (TXE), initiated by 1,3,2-dioxathiolan-2,2-oxide (DTD). The Lewis acidic sulfur in DTD attacked the oxygen atom of TXE, triggering cationic polymerization.[34] As shown in Figure S2, MPN-PTXE completely turned into a solid after 5 h at 60 °C, proving the successful polymerization of TXE. FTIR spectra further confirmed the structural evolution, which are shown in Figure S3. The disappearance of the cyclic ether C−H stretching vibration at 951 cm^{-1} and the emergence of characteristic polyether peaks verified the successful ring-opening polymerization of TXE.[35] Complementary Raman spectroscopy also confirmed the disappearance of the cyclic ether peak at 967 cm^{-1} and the appearance of a chain ether signature at 918 cm^{-1} after polymerization (Figure S4).[36]

https://doi.org/10.1021/jacs.6c07280
J. Am. Chem. Soc. 2026, 148, 24499−24509

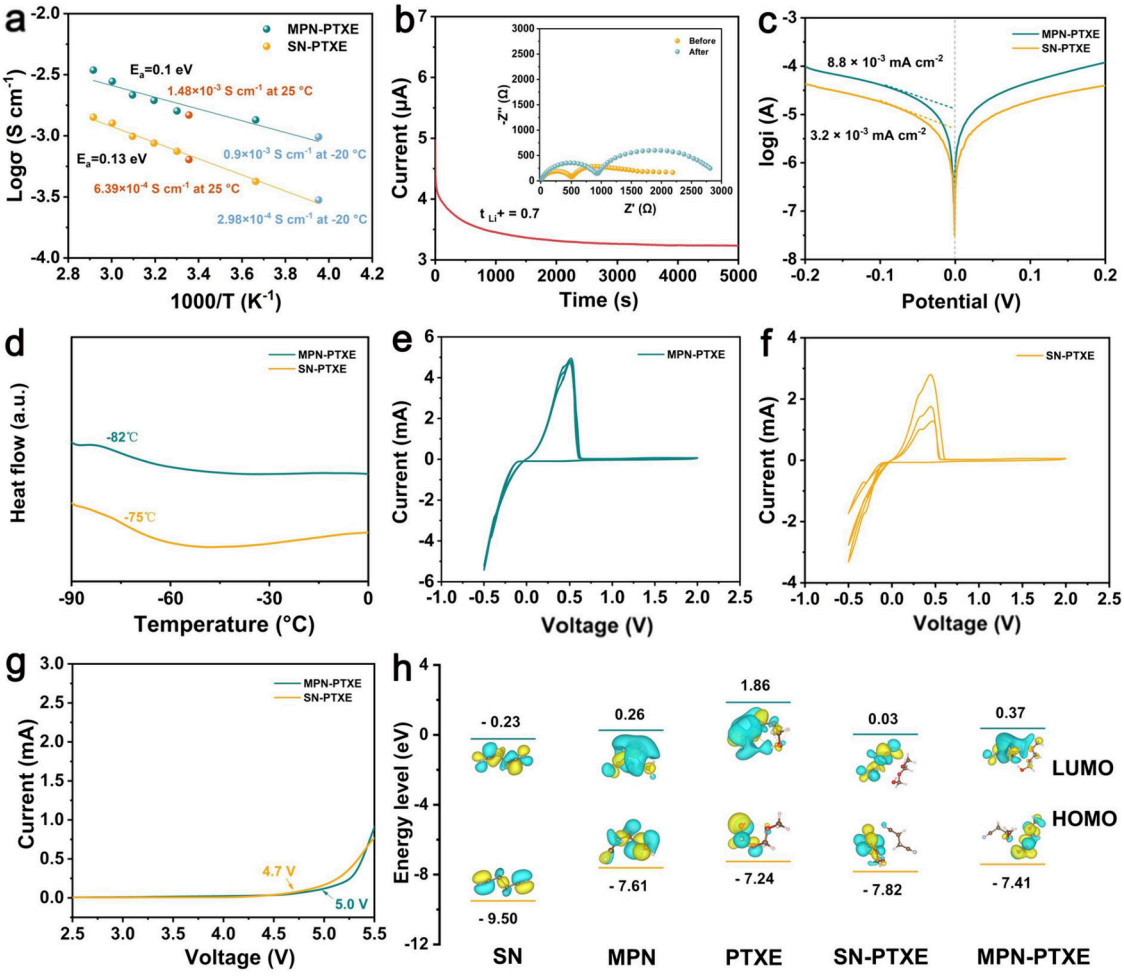

Figure 3. Electrochemical performance analysis at −20 °C. (a) Arrhenius plots of ionic conductivity. (b) Current−time curve of the Li|MPN-PTXE|Li cells at 10 mV (inset shows the EIS curves before and after polarization). (c) Tafel plots for different electrolytes. (d) DSC curves for different electrolytes. (e, f) CV curves for MPN-PTXE and SN-PTXE. (g) LSV curves for different electrolytes. (h) Calculated highest occupied molecular orbital (HOMO) and lowest unoccupied molecular orbital (LUMO) of SN, MPN, PTXE, SN-PTXE, and MPN-PTXE.

Subsequently, the structure and stability of the MPN-PTXE were analyzed. As shown in Figure S5, SEM images revealed that the resulting MPN-PTXE was uniformly embedded within a cellulose framework with a thickness of approximately 50 μm, facilitating efficient Li^+ transport. The enhanced stability of the MPN against the Li metal anode was corroborated by ^1H NMR spectroscopy (Figure 1e), in which the α-hydrogen signal in MPN shifted upfield compared to that in SN, indicating increased electron density and improved stability. Practical compatibility with the Li metal anode was then evaluated. As shown in Figure S6, the MPN-PTXE precursor exhibited a contact angle of 32.4° on Li metal, markedly lower than that of the SN-PTXE (SN-modified PTXE SPE) precursor (52.9°), indicating better wettability and lower interfacial resistance. After standing for 24 h, the SN-PTXE precursor-covered Li metal showed significant polymerization and surface inhomogeneity, whereas the MPN-PTXE interface remained smooth and unchanged, demonstrating superior compatibility (Figure 1f). Additionally, to clarify that SN polymerization rather than TXE polymerization occurred on the Li metal surface, several mixtures including MPN, MPN-TXE, SN-TXE, SN-DME, DME, and DME-TXE were applied to Li metal. As shown in Figure S7, only systems containing SN, i.e., SN-TXE and SN-DME, exhibited polymerization and surface corrosion, while all MPN- and DME-based mixtures maintained a smooth interface without reaction. This confirmed that SN—but not TXE or MPN—readily underwent Li-induced self-polymerization, leading to interfacial degradation and a shortened cycle life of LMBs. SEM observations also provided additional evidence that TXE did not polymerize on the Li metal surface (Figure S8). As demonstrated by the FTIR spectra in Figure S9, the appearance of C═C bonds in SN-TXE further confirmed the instability between SN and Li metal, which promoted the polymerization of SN. Thus, modifying one terminal of SN significantly enhanced the compatibility with the Li metal anode, effectively suppressing detrimental side reactions and the self-polymerization of SN. This molecular design preserved the high oxidation resistance and ionic conductivity while extending the electrochemical stability and improving low-temperature performance, making it a superior plasticizer for in situ polymerized SPEs.

Li^+ Migration Mechanism

To elucidate the mechanisms for the rapid Li^+ migration within the polymer electrolytes and their specific Li^+ solvation structures, molecular dynamics (MD) simulations were conducted. As shown in Figure 2a,d, MD simulation snapshots revealed the interactions between Li^+ and SPEs. Analysis based

https://doi.org/10.1021/jacs.6c07280
J. Am. Chem. Soc. 2026, 148, 24499−24509

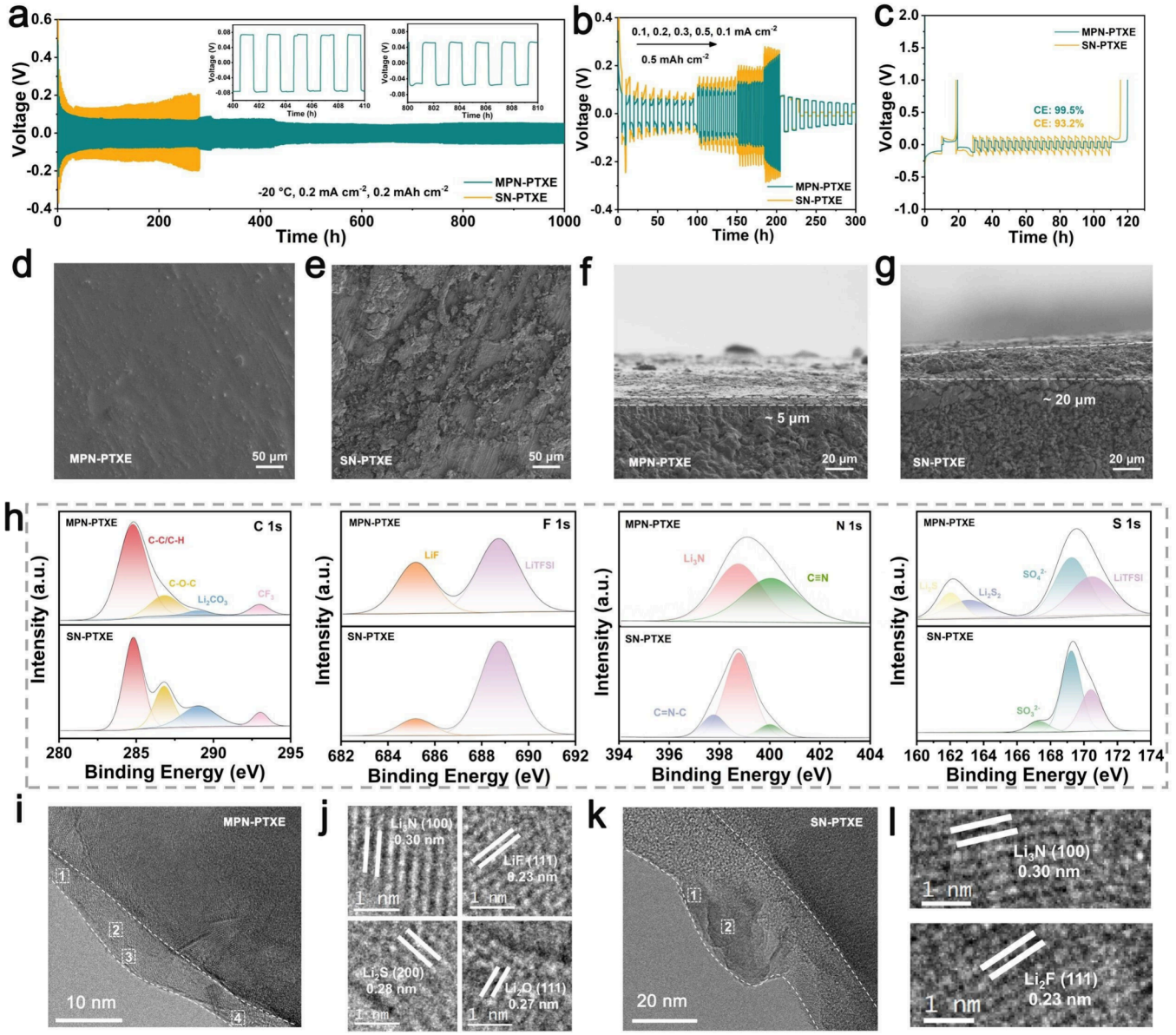

Figure 4. Li deposition/stripping behavior and subsequent analysis at −20 °C. (a) Cycling stability of symmetric cells using SN-PTXE and MPN-PTXE electrolytes at 0.2 mA cm^{-2} and 0.2 mAh cm^{-2}. (b) Rate performance of symmetric cells using SN-PTXE and MPN-PTXE electrolytes. (c) Voltage−time curves of Li|Cu half batteries at 0.5 mA cm^{-2} for calculating the average CEs. (d, e) SEM images of Li anodes after cycling in different SPEs, (d) MPN-PTXE and (e) SN-PTXE. (f, g) SEM images of cross-section of Li metal anode at −20 °C after 50 cycles with different electrolytes, (f) MPN-PTXE and (g) SN-PTXE. (h) XPS spectra of Li metal anodes after cycling with different electrolytes. (i) Cryogenic atomic-resolution TEM image of the SEI formed by MPN-PTXE. (j) HRTEM image of SEI film formed by MPN-PTXE. (k) Cryogenic atomic-resolution TEM image of the SEI formed by SN-PTXE. (l) HRTEM image of SEI film formed by SN-PTXE.

on the radial distribution functions (RDFs) indicated that in the MPN-PTXE SPE, the average coordination numbers of Li^+-N_{MPN} (0.59) and Li^+-O_{MPN} (0.36) were lower than that of Li^+-N_{SN} (1.35). This weak coordination interaction facilitates the desolvation of Li from the solvated shell, thereby lowering the desolvation energy barrier and promoting rapid Li transport (Figure 2b,e). The coordination environments of Li^+ were further probed by Raman spectroscopy, focusing on the symmetric S−N−S stretching mode of $TFSI^-$ around 742 cm^{-1}. Deconvolution of the Raman spectra allows the quantification of distinct $TFSI^-$ species, including free anions, contact ion pairs (CIPs, one $TFSI^-$ coordinated to Li^+), and aggregates (AGGs, multiple $TFSI^-$ coordinated to Li^+), based on their characteristic peak shifts and integrated areas. As shown in Figure 2c,f, in the SN-PTXE SPE, the contact ion pairs (CIPs) and aggregates (AGGs) accounted for 58% and 42%, respectively, while in the MPN-PTXE SPE, the proportions were 47% and 53%, respectively. According to previous reports, a higher proportion of AGGs can promote the formation of an anion-derived, inorganic-rich solid electrolyte interphase (SEI), thereby enhancing the interface stability of the Li metal anode. Furthermore, ^7Li NMR spectroscopy indicated a downfield shift of the ^7Li signal when MPN replaced SN, consistent with weaker Li^+−MPN binding in the MPN-PTXE SPE. This weakened interaction promoted the formation of more AGGs, aligning with the molecular design strategy (Figure S10).

https://doi.org/10.1021/jacs.6c07280
J. Am. Chem. Soc. 2026, 148, 24499−24509

Furthermore, the binding energy of MPN−TFSI$^-$ was −4.7 eV, higher than that of SN−TFSI$^-$ (−4.28 eV), further demonstrating that the introduction of C−H restricts anion mobility and enhances Li^+ kinetics, corresponding to the ESP. (Figure S11). As shown in Figure 2g, these results collectively highlight that enhanced Li^+ mobility and a stable SEI layer are critical for the application of LMBs, particularly at low temperatures.

Electrochemical Characteristics of the MPN-PTXE SPE

Electrochemical impedance spectroscopy (EIS) was first employed to investigate the Li^+ transport behavior from −20 to 70 °C. As shown in Figure S12 and Figure 3a, the ionic conductivity of the SPEs increased with temperature, owing to enhanced polymer chain mobility at elevated temperatures. At room temperature, the MPN-PTXE SPE exhibited a conductivity of 1.48×10^{-3} S cm^{-1}, substantially higher than that of the SN-PTXE SPE (6.39×10^{-4} S cm^{-1}). Notably, even at −20 °C, the MPN-PTXE SPE maintained a high ionic conductivity of 0.9×10^{-3} S cm^{-1}, which enabled the application of LMBs at low temperatures. Furthermore, according to the Arrhenius equation, the activation energy of the MPN-PTXE SPE was 0.1 eV, which was also lower than that of the SN-PTXE SPE (0.13 eV). In the MPN-PTXE system, the ether functional group at the SN terminal weakens Li^+−nitrile coordination, promoting anion (TFSI$^-$) participation in the Li^+ solvation shell. This anion-rich solvation structure shifts the Li^+ migration mechanism from segmental motion of the polymer matrix to structural diffusion via anion exchange, thereby lowering the energy barrier for Li^+ hopping. Concurrently, EIS tests were conducted on symmetric cells with different SPEs at −20 °C, and the corresponding equivalent circuit models were constructed (Figure S13). The results showed that the MPN-PTXE SPE exhibited lower interfacial impedance, which can be attributed to the anion-derived inorganic-rich SEI (as confirmed by the XPS and TEM results in Figure 4) that facilitates rapid interfacial ion transport and significantly reduces interfacial resistance. The Li^+ transference number (t_{Li^+}) is another crucial parameter governing Li^+ transport. A high t_{Li^+} can effectively reduce Li^+ concentration polarization and promote the formation of a stable SEI layer. As shown in Figure 3b and Figure S14, the t_{Li^+} of the MPN-PTXE SPE reached 0.7 at −20 °C, outperforming the SN-PTXE SPE. This result indicated that the ion−dipole interactions between the weakly polar C−H bonds in the MPN molecule and anions in the Li salts can promote the dissociation of Li salts and improve the Li^+ transference number. Furthermore, Tafel polarization curves revealed a higher exchange current density for the MPN-PTXE SPEs compared to the SN-PTXE SPEs, indicating faster interfacial Li^+ transport kinetics essential for the low-temperature operation of LMBs (Figure 3c).

After that, the thermal stability and electrochemical stability of the MPN-PTXE SPE were investigated. As is well-known, reducing the glass transition temperature (T_g) of SPEs generally promotes polymer segment mobility and facilitates Li^+ migration, particularly at low temperatures. As shown in Figure 3d, the T_g of the MPN-PTXE SPE was −82 °C, lower than that of the SN-PTXE SPE (−75 °C), contributing to its superior low-temperature ionic conductivity. Moreover, thermogravimetric analysis (TGA) results demonstrated that the MPN-PTXE SPE possessed improved thermal stability over the SN-PTXE SPE, underscoring the beneficial effect of cyano-ether molecules in enhancing thermal robustness, a critical factor for long-term cycling performance (Figure S15). In contrast, SN not only exhibited inferior thermal stability but also exacerbated the degradation of the electrode−electrolyte interface.

For the electrochemical stability, cyclic voltammetry (CV) curves at different cycle numbers were first analyzed, as shown in Figure 3e,f. It can be seen that the MPN-PTXE SPE revealed excellent interfacial stability, with negligible changes in the CV profiles across cycles. In contrast, the SN-PTXE SPE showed progressive interfacial degradation, as evidenced by emerging reduction peaks and decreasing current responses, which can be ascribed to continuous side reactions between SN and Li metal. Linear sweep voltammetry (LSV) was conducted to evaluate the oxidative stability of the SPEs. As shown in Figure 3g, compared to the SN-PTXE SPE, the electrochemical window of the MPN-PTXE SPE was significantly expanded, with the MPN-PTXE SPE beginning to oxidize at around 4.7 V, while the MPN-PTXE SPE exhibited a higher decomposition voltage of >5.0 V at −20 °C. As evidenced by the XPS spectra in Figure S16, the C≡N bonds in the SN moiety decomposed into C═N—C due to the incompatibility between SN and Li metal, whereas the C≡N bonds in MPN remained relatively stable, demonstrating that introducing ether functional groups at the SN terminal can improve the oxidation stability of MPN. This enhanced oxidative stability of MPN-PTXE arises from two complementary aspects. At the molecular level, although MPN contains an ether-like (−OCH_3) terminal group, the ether oxygen is separated from the nitrile group by a three-carbon chain, resulting in a weaker electron-donating effect, while the electron-withdrawing nature of the —C≡N group remains dominant. This endows MPN with intrinsically favorable electronic properties, as quantitatively corroborated by the highest occupied molecular orbital (HOMO) and lowest unoccupied molecular orbital (LUMO) energy levels calculations discussed next. As shown in Figure 3h, compared to MPN, SN exhibited the lowest LUMO energy value (−0.23 eV), indicating reduced antioxidant stability and a tendency toward side reactions. Additionally, after combining with PTXE, both SN-PTXE and MPN-PTXE exhibited reduced HOMO values, suggesting improved antioxidant properties due to the electron-withdrawing —C≡N group. However, due to the poor reductive stability of SN, it may undergo side reactions with Li metal, hindering the operation of SPEs. In parallel, at the solvation level, the weaker Li^+−MPN coordination promotes an anion-rich solvation environment, which reduces the exposure of solvent molecules at the cathode interface and facilitates the formation of a robust, anion-derived CEI layer rich in inorganic species (such as LiF or Li_3N), as confirmed by XPS in Figure S24. Consequently, the interfacial oxidation is effectively suppressed despite the presence of ether-like functional groups.

Li Plating/Stripping Behavior and Post Analysis

To evaluate the stability of the MPN-PTXE SPE against the Li metal anode during electrochemical cycling, symmetric Li||Li cells were assembled and tested. As shown in Figure 4a, at a current density of 0.2 mA cm^{-2}, the symmetric Li|MPN-PTXE|Li cells can achieve stable cycling over 1000 h while maintaining a low polarization voltage of ∼70 mV. In contrast, the Li|SN-PTXE|Li symmetric cells showed continuously increasing polarization after 200 h, ultimately leading to a

https://doi.org/10.1021/jacs.6c07280
J. Am. Chem. Soc. 2026, 148, 24499−24509

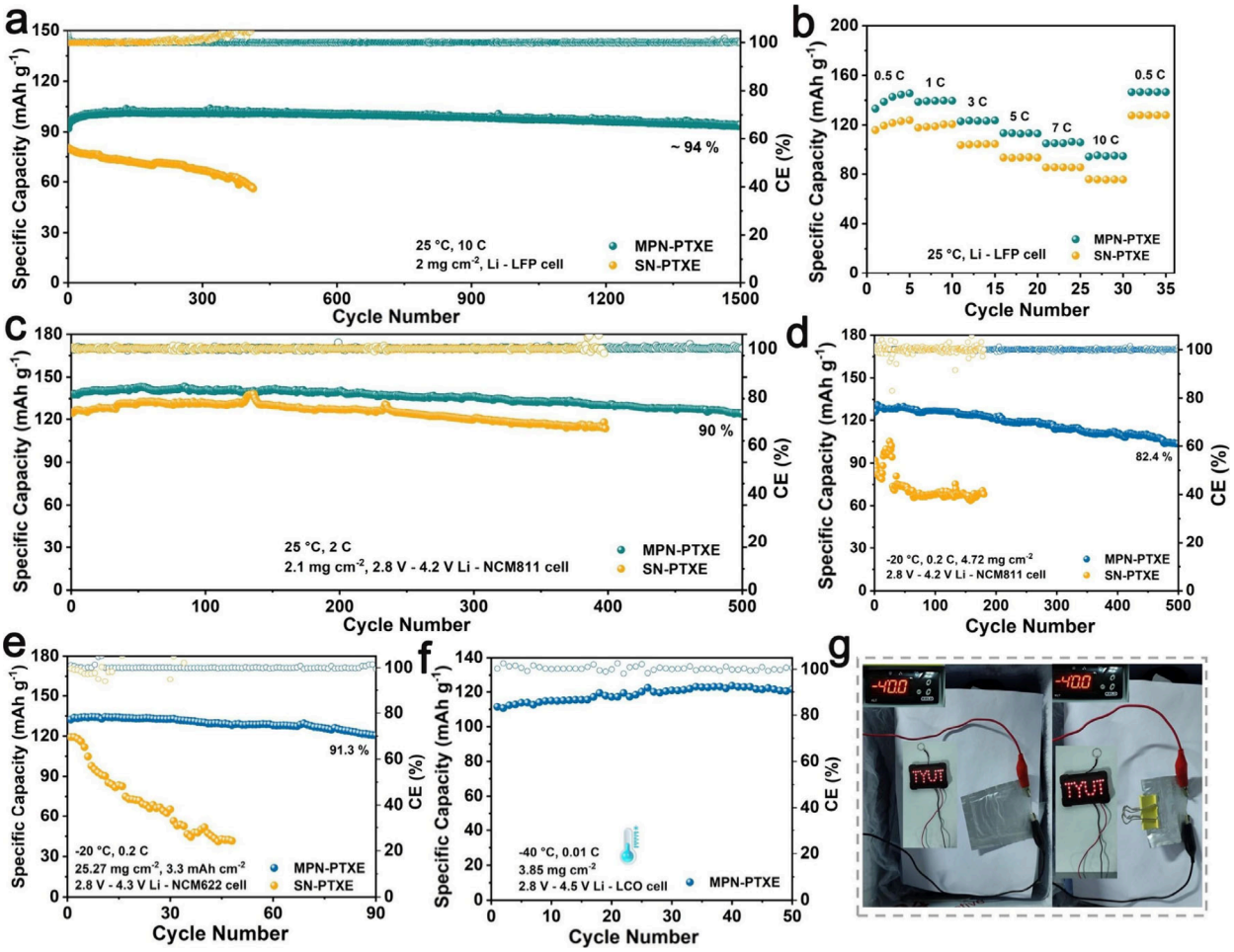

Figure 5. Full cells. (a) Long-cycle performance and (b) rate performance of Li||LFP cells with MPN-PTXE and SN-PTXE electrolytes at room temperature. (c) Cycling performance of Li||NCM811 cells operating at 2.0 C and 25 °C. (d) Cycling performance of Li||NCM811 cells operating at 0.2 C and −20 °C. (e) Cycling performance of Li||NCM622 cells under a high cathode loading of ∼25.27 mg cm^{-2} at 0.2 C and −20 °C. (f) Cycling performance of Li||LCO cells operating at 0.01 C at −40 °C. (g) Pouch cells under normal and folded conditions for LED light panels at −40 °C.

short circuit. Moreover, even at the extreme temperature of −40 °C, the symmetric cells using the MPN-PTXE SPE can also run over 1000 h, underscoring the role of MPN in facilitating rapid Li^+ transport and forming a stable SEI layer (Figure S17). As shown in Figure 4b, at −20 °C, within a current density range of 0.1 to 0.5 mA cm^{-2} and a fixed areal capacity of 0.5 mAh cm^{-2}, the cells using the MPN-PTXE SPE consistently exhibited a lower polarization voltage compared to the cells with the SN-PTXE SPE. Notably, when the current density was reduced from 0.5 to 0.1 mA cm^{-2}, the Li|SN-PTXE|Li symmetric cells experienced a short circuit due to severe interfacial instability, whereas the polarization voltage of the symmetric cells using the MPN-PTXE SPE maintained stable, demonstrating significantly improved reversibility. The structural stability of the MPN-PTXE SPE under electrochemical operation was further evidenced by postcycling Raman analysis. After 50 cycles, the characteristic chain ether peak at 918 cm^{-1} was well preserved with no reappearance of the cyclic ether peak at 967 cm^{-1} (Figure S18a), confirming that no depolymerization occurred during prolonged cycling. Coupled with the stable impedance response observed over 60 cycles (Figure S18b), these results indicate that the MPN-PTXE system maintains its structural and interfacial integrity under dynamic electrochemical conditions. The reversibility of Li plating/stripping was further investigated using Li|Cu half cells. As shown in Figure 4c, the average CE of cells with the SN-PTXE SPE was only 93.2% at −20 °C, while the half cells using the MPN-PTXE SPE delivered a high average CE of 99.5%, indicating superior interfacial compatibility and reduced side reactions. Additionally, the cells using the MPN-PTXE SPE exhibited a lower nucleation overpotential and growth overpotential than those using the SN-PTXE SPE, suggesting enhanced interfacial ion-transfer kinetics, which was beneficial for the run of LMBs at low temperatures (Figure S19).

The surface morphology of the Li metal anode after cycling at −20 °C with different SPEs was investigated by SEM. As shown in Figure 4d,e, the Li metal anode after cycling with the MPN-PTXE SPE displayed a smooth and uniform surface without Li dendrites, whereas the SN-PTXE SPE-based electrode showed irregular and thick deposition. The thickness of the plating/stripping Li layer in the MPN-PTXE SPE-based system was about 5 μm, much thinner than that using the SN-PTXE SPE (∼20 μm (Figure 4f,g). AFM further confirmed the improved morphology: the average surface roughness of the Li metal anode after cycling with the MPN-PTXE SPE was 21.6 nm, significantly lower than that with the SN-PTXE SPE (47.9 nm), confirming the reversibility of Li plating/stripping in the MPN-PTXE SPE (Figure S20).

https://doi.org/10.1021/jacs.6c07280
J. Am. Chem. Soc. 2026, 148, 24499−24509

X-ray photoelectron spectroscopy (XPS) was employed to analyze the SEI layer on the surface of the Li metal anode after cycling at −20 °C. As shown in Figure 4h, the SEI formed with MPN-PTXE SPE was predominantly composed of inorganic species such as LiF, Li_3N, and Li_2S, originating from the decomposition of MPN and $TFSI^-$, which enabled a stable interface and facilitated Li^+ conduction and uniform Li deposition at low temperatures. The peak at ∼685 eV in the F 1s spectrum corresponds to LiF, and the peak at ∼162 eV in the S 1s spectrum corresponds to Li_2S, confirming the formation of an anion-dominated Li^+ solvation structure. In contrast, the SEI layer formed with SN-PTXE SPE lacked sufficient inorganic components due to continuous side reactions between SN and the Li metal anode, resulting in interfacial corrosion and increased impedance.

Further analysis was conducted using cryogenic transmission electron microscopy (cryo-TEM). As shown in Figure 4i−l, a dense and clearly discernible SEI layer with an approximate thickness of ∼6 nm was observable on the Li surface during cycling in the MPN-PTXE electrolyte. High-resolution transmission electron microscopy (HRTEM) images revealed distinct lattice fringes corresponding to Li_2S, LiF, and Li_3N, confirming the formation of inorganic-rich components during long-term electrochemical cycling. By contrast, the Li surface in SN-PTXE exhibited a markedly thicker SEI layer of approximately ∼20 nm. HRTEM imaging confirmed that this SEI contains a small number of inorganic components. This was also consistent with the XPS results.

Full Cells and Low-Temperature Application

To evaluate the practical applicability of the MPN-PTXE SPEs, full cells with $LiFePO_4$ (LFP) and $LiNi_{0.8}Co_{0.1}Mn_{0.1}O_2$ (NCM811) cathodes were assembled. The schematic diagram of their structure is shown in Figure S21, and they were tested at different temperatures. As shown in Figure S22, the Li|MPN-PTXE|LFP full cells demonstrated stable cycling over 1000 cycles at 5.0 C, and the capacity retention rate was >89%, which can be attributed to the high interface stability and stable SEI layer. In contrast, the Li|SN-PTXE|LFP full cells exhibited a low initial discharge capacity and failed after ∼200 cycles due to uncontrolled side reactions between SN and the Li metal anode. When subjected to a higher rate of 10 C (Figure 5a), the Li|MPN-PTXE|LFP full cells maintained a discharge capacity of around 100 mAh g^{-1} and retained nearly 100% of their capacity after 1500 cycles, highlighting their exceptional cycling durability. Furthermore, the rate performance evaluation revealed that the Li|MPN-PTXE|LFP full cells delivered high discharge capacities of 145.4, 139.5, 123.8, 113.1, 105.4, and 94.1 mAh g^{-1} at the rates of 0.5, 1.0, 3.0, 5.0, 7.0, and 10 C, respectively. Upon returning to 0.5 C, the capacity recovered to 146.5 mAh g^{-1}, indicating a highly reversible electrochemical process (Figure 5b and Figure S23).

Subsequently, to verify the high-voltage matching of the MPN-PTXE SPE, the full cells with the NCM811 cathode (cutoff voltage: 4.2 V) exhibited an initial discharge capacity of 137.8 mAh g^{-1} at 2.0 C and retained >90% of their capacity after 500 cycles, demonstrating compatibility with high-voltage cathodes, which once again proved the interface stability of the MPN-PTXE SPE originating from the molecular modification of SN (Figure 5c). Furthermore, XPS was employed to analyze the CEI of Li||NCM811 full cells after 50 cycles. In the C 1s spectra, the peaks corresponding to organic species such as C−O and C═O were weaker for the MPN-PTXE electrolyte. Meanwhile, the F 1s spectra verified that the CEI formed in the MPN-PTXE electrolyte exhibited a significantly higher LiF content, which enhanced the mechanical and chemical stability of the interface. In addition, the N 1s spectra revealed that the CEI derived from the MPN-PTXE system possessed higher contents of C≡N bonds and Li_3N, indicating improved interfacial stability and high-voltage tolerance (Figure S24).

Following closely, we explored the potential applications of MPN-PTXE SPE at low temperatures. As shown in Figure 5d, at −20 °C, the Li|MPN-PTXE|NCM811 full cells delivered a high initial discharge capacity of 125.7 mAh g^{-1} at 0.2 C, maintaining 103.6 mAh g^{-1} after 500 cycles, corresponding to a capacity retention of 82.4%. The small voltage polarization observed between the charge and discharge plateaus indicated low interfacial impedance and rapid ion transport facilitated by the stable SEI layer (Figure S25). In contrast, the full cells using the SN-PTXE SPE suffered from rapid capacity decay (∼70 mAh g^{-1}) and an unstable CE due to severe interfacial side reactions. To achieve a higher energy density, the high-voltage $LiCoO_2$ cathode (cutoff voltage: 4.5 V) was further matched with the SPEs. As shown in Figure S26, at −20 °C, the full cells with MPN-PTXE SPE and the high-voltage $LiCoO_2$ cathode delivered a high discharge capacity of ∼116 mAh g^{-1} after 200 cycles at 0.2 C, with a capacity retention rate of 95.7%. In addition, a cathode with a high mass loading was also used to match with the SPEs. As shown in Figure 5e, under a high loading (∼25.27 mg cm^{-2}), the Li|MPN-PTXE|NCM622 full cells can also exhibit stable cycling over 90 cycles at −20 °C. However, the cells in the control group were unable to run properly. Moreover, even at −40 °C, Li||LCO cells can undergo 50 stable cycles at high capacity (Figure 5f). Furthermore, an extended comparison was conducted with the latest research findings on in situ polymerized electrolytes reported externally. The MPN-PTXE SPE demonstrates distinct advantages across three critical dimensions: rate capability, cycle life, and capacity retention (Figure S27).[37−42] Lastly, a pouch cell was assembled with the MPN-PTXE SPE, and it can successfully power an LED panel even when folded at −40 °C, demonstrating not only excellent low-temperature performance but also remarkable mechanical flexibility and safety (Figure 5g).

CONCLUSION

In summary, this work presented a novel molecular engineering strategy for low-temperature SPEs through the innovative design of a methoxy-functionalized cyano-based plasticizer. By substituting one terminal cyano group in SN with a methoxy moiety, we successfully obtained MPN, which significantly enhanced interfacial stability with the Li metal anode. The introduced methoxy group served as an electron-donating unit that increased the electron density of α-hydrogen, thereby addressing the SN−Li molecular crosstalk problem and lowering the freezing point to −62.9 °C, resulting in enhanced low-temperature kinetics. The resulting MPN-PTXE SPE combined the exceptional Li metal compatibility of ether-based molecules with the high oxidation resistance of cyano-based molecules, enabling stable cycling at high voltages and low temperatures. Thus, the MPN-PTXE SPE demonstrated remarkable electrochemical performance, including a high ionic conductivity of 0.9×10^{-3} S cm^{-1} and a Li^+ transference number of 0.70 at −20 °C. The Li||Li symmetric cell could maintain stable cycling for over 1000 h at −20 °C, while all the full cells (Li||LFP, Li||NCM811, and Li||NCM622) could run

https://doi.org/10.1021/jacs.6c07280
J. Am. Chem. Soc. 2026, 148, 24499−24509

stably at −20 °C and exhibited high capacity retention. This study provided a compelling approach to address the persistent challenge of interfacial instability between the Li metal anode and SN plasticizer in SPEs through selective molecular modulation, offering new prospects for the development of high-energy-density LMBs at low temperatures.

■ ASSOCIATED CONTENT

Supporting Information

The Supporting Information is available free of charge at https://pubs.acs.org/doi/10.1021/jacs.6c07280.

Experimental details; materials and methods; ring-opening polymerization mechanism of TXE; additional data, including optical images, FTIR spectra, Raman spectra, SEM images, contact angle data, ^{7}Li NMR spectra, binding energies, EIS spectra, current−time curve, TG curves, XPS spectra, cycling performance data, AFM images, and charge−discharge curves; and performance comparison with other in situ polymerized electrolytes (PDF)

■ AUTHOR INFORMATION

Corresponding Authors

Lifeng Hou − *College of Materials Science and Engineering, Taiyuan University of Technology, Taiyuan, Shanxi 030024, P. R. China*; Email: houlifeng@tyut.edu.cn

Shi Wang − *State Key Laboratory of Flexible Electronics (LoFE) & Institute of Advanced Materials (IAM), Nanjing University of Posts & Telecommunications, Nanjing, Jiangsu 210023, P. R. China; Yancheng Rouhe Innovative Technology Service Co., Ltd., Yancheng, Jiangsu 224000, P. R. China*; orcid.org/0000-0002-5331-413X; Email: iamshiwang@njupt.edu.cn

Zhong Jin − *State Key Laboratory of Coordination Chemistry, MOE Key Laboratory of Mesoscopic Chemistry, MOE Key Laboratory of High Performance Polymer Materials and Technology, Jiangsu Key Laboratory of Green Energy Catalysis and Intelligent Chemical Engineering, Suzhou Key Laboratory of Green Intelligent Manufacturing of New Energy Materials and Devices, Tianchang New Materials and Energy Technologies Research Center, Institute of Green Chemistry and Engineering, School of Chemistry and Chemical Engineering, Nanjing University, Nanjing, Jiangsu 210023, P. R. China*; orcid.org/0000-0001-8860-8579; Email: zhongjin@nju.edu.cn

Qian Wang − *College of Materials Science and Engineering, Taiyuan University of Technology, Taiyuan, Shanxi 030024, P. R. China*; orcid.org/0000-0001-5161-6241; Email: qianwang0825@pku.edu.cn

Authors

Shuai Liu − *College of Materials Science and Engineering, Taiyuan University of Technology, Taiyuan, Shanxi 030024, P. R. China*

Rujian Fu − *College of Materials Science and Engineering, Taiyuan University of Technology, Taiyuan, Shanxi 030024, P. R. China*

Mengfan Zhao − *College of Materials Science and Engineering, Taiyuan University of Technology, Taiyuan, Shanxi 030024, P. R. China*

Bao Li − *College of Materials Science and Engineering, Taiyuan University of Technology, Taiyuan, Shanxi 030024, P. R. China*

Xueqing Chen − *College of Materials Science and Engineering, Taiyuan University of Technology, Taiyuan, Shanxi 030024, P. R. China*

Complete contact information is available at: https://pubs.acs.org/10.1021/jacs.6c07280

Notes

The authors declare no competing financial interest.

■ ACKNOWLEDGMENTS

This work was supported by the National Natural Science Foundation of China (22402146, 22572140, U24A6002, U25A20628, 22561160129, 22479074, 22475096, 62288102, 52533008), the Funded by the Basic Research Program of Jiangsu (BK20243057) the Beijing Natural Science Foundation Xiaomi innovation joint Foundation (L223011), Young Elite Scientists Sponsorship Program by CAST (2022QNRC001), Shanxi energy Internet research institute (SXEI2023A004), Open Research Fund of Guangdong Advanced Carbon Materials Co., Ltd. (Kargen-2024B0905), the special fund for Science and Technology Innovation Teams of Shanxi Province (202204051001004), the Equipment Pre-Research and Ministry of Education Joint Fund (8091B02052407), the Fundamental Research Program Key Project of Jiangsu Province (BK20253008), the Science and Technology Major Project of Jiangsu Province (BG2024013), the Scientific and Technological Achievements Transformation Special Fund of Jiangsu Province (BA2023037), the Academic Degree and Postgraduate Education Reforming Project of Jiangsu Province (JGKT24_C001), the Key Core Technology Open Competition Project of Suzhou City (SYG2024122), the Open Research Fund of Suzhou Laboratory (SZLAB-1308-2024-TS005), the Chenzhou National Sustainable Development Agenda Innovation Demonstration Zone Provincial Special Open Competition Project (2023sfq11, 2025sfq38), and the Fundamental Research Funds for the Central Universities, Nanjing University International Collaboration Initiative (020514380354), the Yanlong Lake Science and Technology Development Program, and the National Natural Science Foundation of NJUPT (NY223079, NY224119).

■ REFERENCES

(1) Tan, J.; Ma, L.; Yi, P.; Wang, Y.; Li, Z.; Fang, Z.; Li, X.; He, S.; Wang, X.; Ye, M.; et al. Scalable Customization of Crystallographic Plane Controllable Lithium Metal Anodes for Ultralong-Lasting Lithium Metal Batteries. *Adv. Mater.* **2024**, *36*, 2403570.

(2) Xiang, J.; Zhang, Y.; Zhang, B.; Yuan, L.; Liu, X.; Cheng, Z.; Yang, Y.; Zhang, X.; Li, Z.; Shen, Y.; et al. A flame-retardant polymer electrolyte for high performance lithium metal batteries with an expanded operation temperature. *Energy Environ. Sci.* **2021**, *14*, 3510−3521.

(3) Dunn, B.; Kamath, H.; Tarascon, J. M. Electrical energy storage for the grid: a battery of choices. *Science (New York, N.Y.)* **2011**, *334*, 928−935.

(4) Suh, J. H.; Han, S. A.; Yang, S. Y.; Lee, J. W.; Shimada, Y.; Lee, S. M.; Lee, J. W.; Park, M. S.; Kim, J. H. Toward Fast-Charging and Dendritic-Free Li Growth on Natural Graphite Through Intercalation/Conversion on MoS2 Nanosheets. *Adv. Mater.* **2025**, *37*, 414117.

(5) Tu, S.; Zhang, B.; Zhang, Y.; Chen, Z.; Wang, X.; Zhan, R.; Ou, Y.; Wang, W.; Liu, X.; Duan, X.; et al. Fast-charging capability of

graphite-based lithium-ion batteries enabled by Li_3P-based crystalline solid−electrolyte interphase. *Nature Energy* **2023**, *8*, 1365−1374.
(6) Lu, G.; Nai, J.; Luan, D.; Tao, X.; Lou, X. W. Surface engineering toward stable lithium metal anodes. *Science Advances* **2023**, *9*, eadf1550.
(7) Wang, Y.; Zhao, P.-C.; Sun, J.; Liang, J.; Shen, T.; Li, C.-H.; Jin, Z. Titanium−Polyoxometalate Crosslinked Metallo−Supramolecular Polymer as Artificial Interfacial Layer for Highly Persistent and Low−Temperature Tolerant Lithium Metal Batteries. *Angew. Chem., Int. Ed.* **2025**, *64*, e202508224.
(8) Liu, J.; Sun, B.; Zhao, L.; Liu, K.; Demicoli, M.; Song, J. Overcoming the Electrolyte-Derived Interphase Through Sequential Reactions for Stable Lithium Metal Anode. *J. Am. Chem. Soc.* **2025**, *147*, 21885−21895.
(9) Zhang, Z.; Lee, J. K. J.; Li, Y.; Zhou, W.; Wu, G.-H.; Lyu, H.; Wan, J.; Chen, H.; Huang, W.; Ye, Y.; et al. Resolving three-dimensional nanoscale heterogeneities in lithium metal batteries with cryoelectron tomography. *Matter* **2025**, *8*, 102266.
(10) Liu, S.; Gu, B.; Chen, Z.; Zhan, R.; Wang, X.; Feng, R.; Sun, Y. Suppressing dendritic metallic Li formation on graphite anode under battery fast charging. *Journal of Energy Chemistry* **2024**, *91*, 484−500.
(11) Han, X.; Mao, S.; Wang, Y.; Lu, Y.; Wang, D.; Sun, Y.; Zheng, Y.; Feng, X.; Lu, L.; Hua, J.; et al. Manipulation of lithium dendrites based on electric field relaxation enabling safe and long-life lithium-ion batteries. *Nat. Commun.* **2025**, *16*, 3699.
(12) He, C.; Ying, H.; Cai, L.; Chen, H.; Xu, Z.; Liu, S.; Huang, P.; Zhang, H.; Song, W.; Zhang, J.; et al. Tailoring Stable PEO-Based Electrolyte/Electrodes Interfaces via Molecular Coordination Regulating Enables 4.5 V Solid-State Lithium Metal Batteries. *Adv. Funct. Mater.* **2024**, *34*, 2410350.
(13) Qin, M.; Zeng, Z.; Wu, Q.; Ma, F.; Liu, Q.; Cheng, S.; Xie, J. Microsolvating Competition in Li^+ Solvation Structure Affording PC-Based Electrolyte with Fast Kinetics for Lithium-Ion Batteries. *Adv. Funct. Mater.* **2024**, *34*, 2406357.
(14) Liu, S.; Wu, B.; Bai, X.; Zhang, J.; Chang, X.; Hou, L.; Huang, H.; Wei, Y.; Wang, S.; Jin, Z.; et al. A Solvent-Induced Solid Polymer Electrolyte with Controllable Polymerization for Low-Temperature Lithium Metal Batteries. *Nano Lett.* **2025**, *25*, 5241−5249.
(15) Liang, Z.; Liu, C.; Bai, X.; Zhang, J.; Chang, X.; Zhang, B.; Xia, M.; Du, H.; Huang, H.; Wu, B.; et al. Integrating Competitive Li^+ Coordination with Immobilized Anions in Composite Solid Electrolyte for High-Performance Li Metal Batteries. *Advanced Science* **2025**, *12*, 2413875.
(16) Zhang, W.; Lu, Y.; Feng, Q.; Wang, H.; Cheng, G.; Liu, H.; Cao, Q.; luo, Z.; Zhou, P.; Xia, Y.; et al. Multifunctional electrolyte additive for high power lithium metal batteries at ultra-low temperatures. *Nat. Commun.* **2025**, *16*, 3344.
(17) Lu, P.; Zhou, Z.; Xiao, Z.; Lu, J.; Zhang, J.; Hu, G.; Yan, W.; Xia, S.; Zhang, S.; Wang, Z.; et al. Materials and chemistry design for low-temperature all-solid-state batteries. *Joule* **2024**, *8*, 635−657.
(18) Chen, X.; Qin, C.; Chu, F.; Li, F.; Liu, J.; Wu, F. Contriving a gel polymer electrolyte to drive quasi-solid-state high-voltage Li metal batteries at ultralow temperatures. *Energy Environ. Sci.* **2025**, *18*, 910−922.
(19) Wang, S.; Zhang, L.; Zeng, Q.; Guan, J.; Gao, H.; Zhang, L.; Zhong, J.; Lai, W.-Y.; Wang, Q. Designing Polymer Electrolytes via Ring-Opening Polymerization for Advanced Lithium Batteries. *Adv. Energy Mater.* **2024**, *14*, 2302876.
(20) Sun, Z.; Yang, J.; Wu, Y.; Meng, F.; Niu, Y.; Xu, H.; Zhu, Y.; Hong, B.; Chen, Z.; Zhu, J.; et al. Stabilizing Residual Monomers within In Situ Polymerized Electrolytes for High-Voltage Lithium Metal Batteries. *J. Am. Chem. Soc.* **2025**, *147*, 18064−18073.
(21) Rui, X.; Hua, R.; Ren, D.; Qiu, F.; Wu, Y.; Qiu, Y.; Mao, Y.; Guo, Y.; Zhu, G.; Liu, X.; et al. In Situ Polymerization Facilitating Practical High-Safety Quasi-Solid-State Batteries. *Adv. Mater.* **2024**, *36*, 2402401.
(22) Wu, J.-F.; Wang, Z.; Jin, J.; Kong, Z.-X.; Chen, S.; Liu, J. High-Rate 4.2 V Solid-State Potassium Batteries by In Situ Polymerized Epoxide Ether Electrolyte. *Nano Lett.* **2025**, *25*, 635−640.
(23) Tian, H.; Hong, Z.; Fang, Z.; Luo, Y.; Wu, H.; Zhao, F.; Li, Q.; Fan, S.; Wang, J. 1,8-Diazabicyclo[5.4.0]undec-7-ene as Cyclic Ether Electrolyte Polymerization Inhibition for Wide-Temperature-Range High-Rate Lithium-ion Batteries. *Advanced Science* **2025**, *12*, 2409259.
(24) Xu, H.; Mi, J.; Ma, J.; Han, Z.; Lv, S.; Chen, L.; Zhang, J.; Yang, K.; Li, B.; Li, Y.; et al. Mg^{2+} initiated in situ polymerization of dioxolane enabling stable interfaces in solid-state lithium metal batteries. *Energy Environ. Sci.* **2025**, *18*, 4231−4240.
(25) Liu, Y.; Zou, H.; Huang, Z.; Wen, Q.; Lai, J.; Zhang, Y.; Li, J.; Ding, K.; Wang, J.; Lan, Y.-Q.; et al. In situ polymerization of 1,3-dioxane as a highly compatible polymer electrolyte to enable the stable operation of 4.5 V Li-metal batteries. *Energy Environ. Sci.* **2023**, *16*, 6110−6119.
(26) He, W.; Liu, Z.; Zhang, H.; Liu, S.; Feng, Z.; Ye, J. "Gel-in-Resin" Multifunctional Electrolytes for Enhanced Electrochemical and Mechanical Performance in Lithium-Ion Structural Battery Composites. *Adv. Funct. Mater.* **2026**, *36*, No. e07493.
(27) Ye, X.; Fu, H.; Zhang, Y.; Wu, D.; Zhong, Y.; Wang, X.; Ouyang, X.; Tu, J. Modulating the Li-Ion Transport Pathway of Succinonitrile-Based Plastic Crystalline Electrolytes for Solid-State Lithium Metal Batteries. *Adv. Funct. Mater.* **2025**, *35*, 2413205.
(28) Su, C.; Qu, Y.; Hu, N.; Wang, L.; Song, Z.; Pei, M.; Mao, R.; Jin, X.; Liu, D.; Jian, X.; et al. Rapid Na^+ Transport Pathway and Stable Interface Design Enabling Ultralong Life Solid-State Sodium Metal Batteries. *Angew. Chem., Int. Ed.* **2025**, *64*, No. e202418959.
(29) Zhang, D.; Liu, Y.; Sun, Z.; Liu, Z.; Xu, X.; Xi, L.; Ji, S.; Zhu, M.; Liu, J. Eutectic-Based Polymer Electrolyte with the Enhanced Lithium Salt Dissociation for High-Performance Lithium Metal Batteries. *Angew. Chem., Int. Ed.* **2023**, *62*, e202310006.
(30) Yang, T.; Lou, J.; Hu, L.; Liu, Q.; Huang, Z.; Zhou, Q.; Zhang, H.; Song, W.; Huang, H.; Wang, Y.; et al. In Situ Construction of LiF/Li_3N/Li_xGa Hybrid SEI to Boost Long-Lifespan Succinonitrile-Based Solid-State Lithium Metal Batteries. *Adv. Funct. Mater.* **2025**, *35*, 2423719.
(31) Wang, H.; Yang, J.; Xu, X.; Geng, J.; Lin, X.; Xu, H.; Huang, Y. Competitive Ion Coordination in Gel Polymer Electrolytes Enables Decoupling of Mechanical Strength and Ionic Conductivity. *Adv. Mater.* **2025**, *n37*, No. e04625.
(32) Luo, C.; Ning, C.; Huang, X.; Zhang, P.; Yang, L.; Wang, S.; Wang, J.; Wang, Y.; Wan, K.; Guo, Z. H.; et al. Molecular Engineering of Weakly Solvating Dinitrile Electrolytes for Long-Lasting Room-Temperature Lithium Metal Batteries. *Angew. Chem., Int. Ed.* **2025**, *64*, e202507051.
(33) Fang, R.; Ma, S.; Ding, L.; Gu, Y.; Dong, X.; Si, D. H.; Tian, J. H.; Lin, X. M.; Mao, B. W.; Li, J. F. Lewis-Base Electrolyte Additive Mediates Interfacial Chemistry for Stable Lithium Metal Batteries. *Angew. Chem., Int. Ed.* **2025**, *64*, No. e202502048.
(34) Zhao, J.; Li, M.; Su, H.; Liu, Y.; Bai, P.; Liu, H.; Ma, L.; Li, W.; Sun, J.; Xu, Y. In Situ Fabricated Non-Flammable Quasi-Solid Electrolytes for Li-Metal Batteries. *Small Methods* **2023**, *7*, 2300228.
(35) Yu, M.; Ma, J.; Dong, L.; Huang, M.; Xue, B.; Sun, Y.; Xiang, H. Stabilizing the SiO_x Anode by a Highly Elastic Quasi-Solid Polyether-Based Electrolyte via an In Situ Fabrication. *ACS Appl. Mater. Interfaces* **2025**, *17*, 14097−14108.
(36) Li, Z.; Yu, R.; Weng, S.; Zhang, Q.; Wang, X.; Guo, X. Tailoring polymer electrolyte ionic conductivity for production of low-temperature operating quasi-all-solid-state lithium metal batteries. *Nat. Commun.* **2023**, *14*, 482.
(37) Xu, N.; Song, X.; Sun, G.; Zhang, J.; Quan, Z.; Lou, G.; Li, A.; Li, C.; Zhang, H.; Chen, Y. Over 500 Wh kg^{-1} Solid-State Lithium Metal Batteries with Long Cycling Stability Using In Situ Polymerized Electrolyte. *J. Am. Chem. Soc.* **2026**, *148*, 2471−2480.
(38) Lu, Y.; Liu, Y.; Zhang, S.; Wu, Y.; Cheng, H.; Lu, Y. Toward practical lithium metal batteries via a solvation structure regulation strategy in in situ polymerized fluorinated gel polymer electrolytes. *Energy Environ. Sci.* **2025**, *18*, 9512−9523.
(39) Liu, Q.; Dan, Y.; Niu, Y.; Li, G. Molecular design for in-situ polymerization of hybrid polymer electrolyte enables high-voltage and

https://doi.org/10.1021/jacs.6c07280
J. Am. Chem. Soc. 2026, 148, 24499−24509

high-energy-density quasi-solid-state lithium metal batteries. *Energy Storage Materials* **2025**, *78*, 104277.
(40) Li, J.; Li, C.; Yao, Y.; Li, Z.; Yao, J.; Luo, L.; Liao, W.; Ye, X.; Dai, W.; Li, F.; et al. In Situ Polymerized Flame-Retardant Crosslinked Quasi Solid-State Electrolytes for High-Voltage Lithium Metal Batteries. *Adv. Energy Mater.* **2024**, *14*, 2402362.
(41) Karanth, P.; Weijers, M.; Lavrinenko, A. K.; Izelaar, B.; Kortlever, R.; Ganapathy, S.; Wagemaker, M.; Mulder, F. M. Designing Fluorine-Free Electrolytes for Lithium Metal Batteries. *J. Am. Chem. Soc.* **2025**, *147*, 46008−46022.
(42) Jia, Z.; Wang, F.; Ren, J.; Zhu, J.; Li, H.; Liang, Y.; An, X.; Liu, X.; Sun, X.; Wang, X.; et al. Ultra-Stable Polycarbonate-Based Solid-State Lithium Metal Batteries Enabled by In Situ Polymerized Ferroelectric Engineering. *Adv. Funct. Mater.* **2026**, *36*, e27353.

https://doi.org/10.1021/jacs.6c07280
J. Am. Chem. Soc. 2026, 148, 24499−24509